Effects of freezing, growth, and ice cover on gas transport processes in laboratory seawater experiments

B. Loose,[1] W. R. McGillis,[1] P. Schlosser,[1] D. Perovich,[2] and T. Takahashi[1]

[1] Gas exchange through sea ice is a determining factor in the polar ocean budget of climatically-active gases. We use SF_6 and O_2 as conservative gas tracers to observe transport between the water, ice and air during conditions of freezing and partial ice cover in artificial seawater. During ice growth, O_2 and SF_6, as non-polar solutes, were rejected from the ice into the underlying water at a faster rate than that observed for salt. Measurements of the gas exchange rate, k, through partial ice cover exceeded that expected from linear scaling between 100% open water ($k_{100\%}$) and complete ice cover: at 15% open water, k was 25% of $k_{100\%}$. These results indicate that the net flux of gas through the ice pack may not scale linearly with open water area, as circulation processes under the ice affect the gas exchange rate. **Citation:** Loose, B., W. R. McGillis, P. Schlosser, D. Perovich, and T. Takahashi (2009), Effects of freezing, growth, and ice cover on gas transport processes in laboratory seawater experiments, *Geophys. Res. Lett.*, *36*, L05603, doi:10.1029/2008GL036318.

1. Introduction

[2] During freezing of seawater dissolved solutes (ions and gases) are excluded from the ice crystal structure [*Richardson*, 1976], producing a cascade of processes that affect the circulation and the biogeochemistry of the polar oceans [*Arrigo and Van Dijken*, 2007]. The exclusion of salt produces convection beneath sea ice to such an extent that the mixed layer depth is determined by the amount of sea ice growth during austral winter [*Martinson*, 1990]. Hypersaline brine carves a porous structure within sea ice that is permeable to both water and gas [*Golden et al.*, 2007; *Gosink et al.*, 1976]. As the sea ice temperature decreases, brine becomes further concentrated and carbonate minerals, such as ikaite ($CaCO_3 \cdot 6H_2O$), can precipitate from the solution [*Dieckmann et al.*, 2008; *Marion*, 2001] decreasing carbonate alkalinity. It has been proposed that the loss of carbonate alkalinity can enhance the partial pressure of CO_2 (pCO_2) within the sea ice matrix [*Papadimitriou et al.*, 2003]. These processes, as well as diffusion and air-sea gas transfer, may result in a net redistribution of inorganic carbon from the surface ocean to the atmosphere and to the ocean interior [*Nomura et al.*, 2006; *Rysgaard et al.*, 2007].

[3] This study attempts to isolate the physical processes that can produce mass transport from the biogeochemistry of seawater freezing. The temporal evolution of two aqueous gas tracers, SF_6 and O_2, are measured in comparison with the salt budget under abiotic, conservative, windless conditions. We examine the influence of unconsolidated ice crystal formation and the growth of columnar sea ice. Results are presented indicating that gas is rejected more efficiently than salt from the freezing interface, possibly by differential diffusion rates. We present measurements of gas exchange that show an enhancement in the gas exchange rate through partial ice cover for both O_2 and SF_6. Finally, considering the mechanisms of turbulence production beneath sea ice, we attempt to connect these results with the variation in gas exchange produced by variable turbulence.

2. Methods

[4] A total of six freezing experiments were conducted in a variable temperature cold room at the US Army Corps of Engineers Cold Regions Research and Engineering Laboratory (CRREL) in Hanover, NH. Two gas exchange tanks of different volume were used: a 144 L polypropylene drum (d × h = 49.2 × 75 cm) with a lid and rubber gasket, and a 55 L PVC tank with a lid and O-ring seal (Figure 1). In the 144 L tank, salinity, temperature and pressure were measured using a Seabird SB37SIP CTD probe. Dissolved O_2 concentration was measured using an Aandera Instruments 3830 Optode. Three Rule 360 bilge pumps were used to mix the tank and to circulate water through a length of Tygon tubing for discrete SF_6 sample collection. A similar configuration was used within the 55 L tank.

[5] Before each experiment, artificial seawater was prepared by mixing MilliQ water with sea salt for aquariums (Instant Ocean, Spectrum Brands) to obtain salinity between 33 and 35 psu, as verified with a conductivity probe. Prior to introducing the water mixture, the experiment tanks, instruments and tubing were cleaned with 10% bleach solution to minimize the growth of bacteria. To initiate an experiment, the cold room was set to a temperature between −5 and −20°C, and the seawater bath was allowed to cool (see Table S1 of the auxiliary material for more detail on each experiment).[1] As the water temperature decreased below 5°C, the bath was bubbled with air, for O_2 evasion, or with N_2 for O_2 invasion. Prior to achieving 0°C, aeration was suspended to make estimates of k, before the onset of freezing. Subsequently, ca. 10^{-7} moles of SF_6 were added as a concentrated solution dissolved in 5 ml of freshwater, and the solution was allowed to mix entirely. Water samples for SF_6 were collected with 50 ml glass syringes and

---

[1]Lamont-Doherty Earth Observatory of Columbia University, Palisades, New York, USA.
[2]U.S. Army Corps of Engineers Cold Regions Research and Engineering Laboratory, Hanover, New Hampshire, USA.
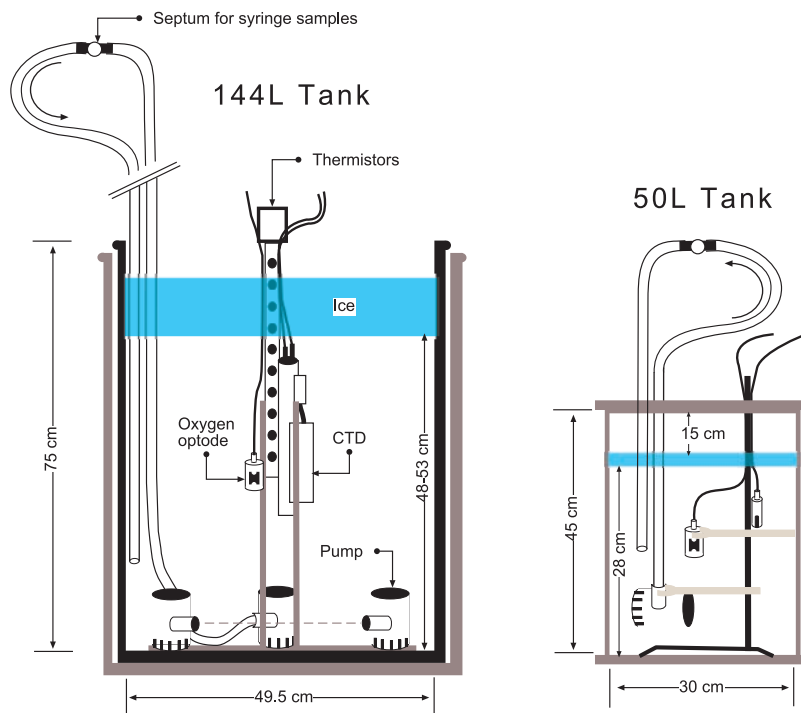
Figure 1. Configuration of instruments in the 144 L and 50 L gas exchange tanks.

needles. The gases were separated using the headspace method [*Wanninkhof et al.*, 1987] and analyzed by gas chromatography as described by *Ho et al.* [1997].

[6] Gas exchange was calculated using the control volume approach. Before each experiment the water was conditioned to enhance the partial pressure gradient between water and air. For SF_6, the gas evasion method was used [*Ho et al.*, 1997]. For O_2, both evasion and invasion were used during successive experiments. For a cylindrical tank of depth (h), the gas exchange rate (k) can be estimated from the initial and final concentration (C_i and C_f) as, k = $h(\Delta t)^{-1}\ln[(C_i - C_{EQ})/(C_f - C_{EQ})]$. C_{EQ} = ßX, where ß is the Bunsen solubility coefficient (volume of gas/volume of water) and X is the volume of pure gas per volume of air.

3. Results and Discussion

3.1. Onset of Freezing

[7] The onset of freezing is evident in both the temperature and O_2 concentration. In the 55 L tank (Figure 2, Expt. 2 and 6) the temperature decreased below the expected freezing point (dashed line) by 0.08 to 0.14 °C, before exhibiting an increase in temperature, followed by an increase in O_2 concentration, which coincided with the rapid appearance of unconsolidated ice crystals in the upper 2–3 cm of the tank. As freezing progressed during Expt. 2, the aqueous O_2 concentration increased, reflecting gas and solute rejection. The slower cooling rate during Expt. 6 caused partial ice cover to persist, following the first onset of freezing, so that the aqueous O_2 concentration continued to decrease beyond 0.1 days.

3.2. Columnar Ice Growth and Solute Rejection

[8] The response of salinity and O_2 to freezing can be compared by normalizing the change of each solute mea-

sured in the water, during an equivalent time interval: $d\overline{O}_2$ = dO_2/O_2 and $d\overline{S}$ = dS/S. During the growth of consolidated ice (Figure 2b, t ≤ 1 days), $d\overline{O}_2$ and $d\overline{S}$ converge and become nearly identical as ice growth tapers off, near t = 1.1 days. Throughout the period of ice growth, the magnitude of $d\overline{O}_2$ exceeded $d\overline{S}$. The same holds true for the period of relatively constant ice thickness (t = 3 – 5 days). Whereas in the absence of ice growth or melt, $d\overline{O}_2$ and $d\overline{S}$ should be almost zero, they are slightly positive indicating residual brine drainage. To compare $d\overline{O}_2$ and $d\overline{S}$ during successive experiments, we fit a linear trend line to the normalized salinity and O_2 time series, during a period of constant ice growth. The magnitude of the slope reflects the normalized rate of change of each parameter. The observations indicate that $d\overline{O}_2$ exceeded $d\overline{S}$ by 20 – 80%. The same effect was observed when comparing the normalized increase in SF_6 during rapid ice growth. The values of $d\overline{O}_2$, $d\overline{S}$, and $d\overline{SF}_6$, and the R^2 coefficients of each fit are listed in Table 1.

[9] To quantify the partitioning of gases between the water and ice, we compared the mass of solute rejected during an interval of ice growth (M_R) to the total mass of solute that was initially in the volume of water that has been frozen (M_{ICE}). This can be calculated by differencing the solute concentration over a short period (S_I, and S_F), and by estimating the decrease in water volume. We define the term rejection ratio (R) as $M_R/M_{ICE} = V_T(\rho_F S_F - \rho_I S_I)/(V_{ICE}\rho_I S_I)$. ρ_F and ρ_I are the initial and final density of the water, V_T is the volume of the tank after freezing has taken place, and V_{ICE} is the water equivalent of the frozen ice. To minimize the effects of gas diffusion through the ice we restrict the calculation to a period less than two days. For constant growth of 4.5 cm of ice during Expt. 3 the salt rejected (M_R) is 143 g. This value is within 12% of the estimated salt rejection using the empirical equations of *Cox and Weeks* [1983] (126 g), who use air temperature and ice growth rate
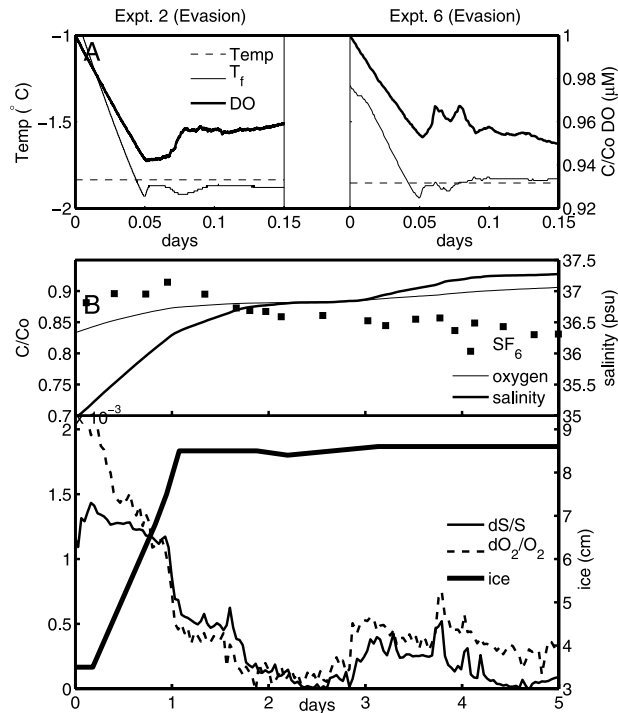
Figure 2. (a) The onset of freezing produces unconsolidated ice crystals and an oscillation in temperature and dissolved O_2, such as during Experiments 2 and 6. The O_2 concentration is normalized by its initial concentration (C_o). T_f indicates the freezing point, which depends on the initial salinity in the tank. (b) Salinity, dissolved oxygen and SF_6 during ice growth and constant ice thickness of 8.6 cm, during Expt. 5, an O_2 invasion and SF_6 evasion experiment. The normalized change in oxygen (dO_2/O_2) and the normalized change in salinity (dS/S) reflect the rate of solute rejection during the different ice formation conditions.

to calculate solute rejection and brine volume. This produces a rejection ratio for salt (R_S) of 45%. The same relationship, applied to dissolved O_2 results in a rejection ratio (R_{O2}) of 61%. A similar calculation for relatively

constant growth conditions during Expt. 5 produces values for R_S of 40% and R_{O2} of 45%. The agreement between the measured mass of rejected salt (M_R) and the result using the method by *Cox and Weeks* [1983] was within 22%. The rate of ice growth is a strong determining factor for the rate of salt rejection, [*Cox and Weeks*, 1983] - the faster the growth rate the larger the amount of salt that remains included in the ice. During Expt. 3 the ice growth rate was 2.56×10^{-5} cm s^{-1}, ~40 % of the growth rate during Expt. 5 (6.47×10^{-5} cm s^{-1}). These results indicate that $39 - 55$ % of the O_2 within the unfrozen water remained included within the sea ice, dissolved within the brine or nucleated into gas bubbles [*Craig et al.*, 1992].

3.3. Gas Exchange Rate During Partial Ice Cover

[10] During Expts. 1, 3, 4 and 5 in the 144 L tank, ice was removed from the surface by drilling holes to measure the rate of gas exchange during partial ice cover. Once a constant fraction of open water was established, the rate of gas exchange was measured for a period of $8 - 20$ hours, using the control volume approach as described in the methods section [*Ho et al.*, 1997]. During these periods the ice thickness remained constant, and residual brine drainage was minimal. Because the O_2 concentration in brine was not measured, a correction for brine drainage was not attempted. However the increase in salinity was less than 0.5% during each measurement period. If the O_2 in brine is proportional to salinity, then brine expulsion would produce a source of O_2 that is less than 5% of the change in O_2 observed during each estimate period, resulting in a 7% difference in k. This 7% bias has been added to the standard error in k, which ranges between 10 and 80%, as indicated by the error bars in Figure 3. Similarly, the change in water volume produced by brine drainage accounts for ~0.1 − 0.3% bias in k.

[11] To evaluate the tendency of gas exchange rate with an increasing fraction of open water, the measurements of k_{O2} and k_{SF6}, normalized by the gas exchange rate at 100% open water ($k_{100\%}(O_2) = 1.02$ and $k_{100\%}(SF_6) = 0.83$ cm h^{-1}), are plotted versus the fraction of open water surface in Figure 3 (see Figure S1 of the auxiliary material

Table 1. Comparison of the Normalized Change in Salinity ($d\overline{S}$) With the Normalized Changes in O_2 ($d\overline{O}_2$) and SF_6 ($d\overline{SF}_6$), Measured Beneath the Ice During Conditions of Constant, Rapid Ice Growth[a]

	Experiment 1	Experiment 3	Experiment 5	Experiment 6
Temp 5 cm above ice (°C)	−5	−13	−8	−7.5
Growth rate (cm s^{-1})	1.53×10^{-5}	2.56×10^{-5}	6.47×10^{-5}	N/A
dS, S (psu)	1.8, 35.5	0.6, 40.3	1.1, 35.5	3.3, 34
R^2 (dS)	0.84	0.98	0.97	0.99
$d\overline{S}$	0.05	0.02	0.03	0.10
dO_2, O_2 (mmol L^{-1})	27.7, 350.0	2.0, 74.0	6.5, 148.0	N/A
R^2 (dO_2)	0.69	0.99	0.99	N/A
$d\overline{O}_2$	0.08	0.03	0.04	N/A
dSF_6, SF_6 (pmol L^{-1})	N/A	N/A	11.6, 240.0	25.5, 210.0
R^2 (dSF_6)	N/A	N/A	0.74	0.60
$d\overline{SF}_6$	N/A	N/A	0.05	0.12
$d\overline{O}_2$:$d\overline{S}$	1.6	1.8	1.5	N/A
$d\overline{SF}_6$:$d\overline{S}$	N/A	N/A	1.6	1.2

[a]$d\overline{S}$, $d\overline{O}_2$ and $d\overline{SF}_6$ reflect the change during a period of one day. The ratios of $d\overline{O}_2$:$d\overline{S}$ and $d\overline{SF}_6$:$d\overline{S}$ greater than 1 indicate that the dissolved gases increased in concentration more rapidly than salinity.
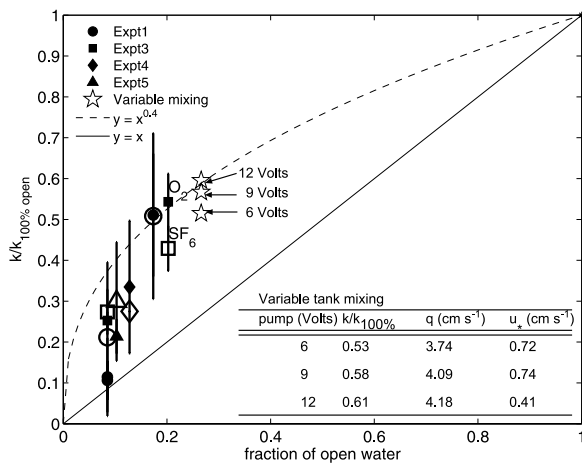
Figure 3. The normalized gas exchange rate ($k/k_{100\%}$) during partial ice cover in these experiments plotted versus the surface area fraction of open water in the 144 L tank. k_{SF6} is plotted in red and k_{O2} in blue. The solid line delineates the 1:1 proportionality between normalized k and the fraction of open water, and the dashed line indicates a power law relationship between k and open water fraction. The open diamonds indicate different mixing rates, produced by varying the voltage of the submersible pumps. Mixing rate is reflected in the scalar turbulent quantities, $q = (\langle u'^2 \rangle + \langle v'^2 \rangle + \langle w'^2 \rangle)^{1/2}$ and $u_* = (\langle u'w' \rangle^2 + \langle v'w' \rangle^2)^{1/4}$, and the table includes these values as well as $k/k_{100\%}$ during 26% partial open water.

for more detail on $k_{100\%}(O_2)$ and gas exchange prior to freezing). The expectation is for $k/k_{100\%}$ to range proportionally between $k/k_{100\%} = 0$ (or the rate of gas diffusion through ice) when there is no open water, and $k/k_{100\%} = 1$ at 100% open water. Without exception, the measurements are clustered above the 1:1 line, exhibiting a tendency that is in excess of the proportional scale. At 15% ice cover, k is 25% of $k_{100\%}$.

[12] The existence of a lead, or opening in the ice pack, can establish several modes of circulation in the water column underneath the ice. In the limit of zero horizontal current motion between the sea ice and the water column, the production of dense water at the ice opening induces free convection that draws water from beneath the adjacent ice in a cellular circulation pattern [*Morison et al.*, 1992]. At the other extreme, motion of the water relative to the ice produces boundary layer turbulence that entrains dense water from the ice opening into the lateral turbulent flow. *Morison et al.* [1992] define the turbulent lead number, or ratio of the buoyancy production to shear production beneath the lead to characterize this spectrum of flow conditions. A lead number less than one describes a condition dominated by boundary layer turbulence, while a lead number greater than one indicates free convection. In both extremes, the existence of lateral flow towards the opening can affect a relatively large heat and mass transfer within the water column relative to the size of the lead opening.

[13] During these measurements of gas exchange under partial ice cover, turbulence was produced via mixing from the submersible pumps, as well as brine-driven buoyant

convection (Figure 2) and heat-loss at the opening. To measure the turbulent mixing during partial ice cover, an Acoustic Doppler Velocimeter (ADV) was submerged 15 cm beneath the ice surface, during one experiment and turbulence intensity was varied by decreasing the submersible pump voltage during conditions of 26% open water fraction. The ADV was set to sample at 25 Hz [*Zappa et al.*, 2003] to compute the scalar quantities, q, proportional to the turbulent kinetic energy and u_*, proportional to the Reynolds stress as $q = (\langle u'^2 \rangle + \langle v'^2 \rangle + \langle w'^2 \rangle)^{1/2}$ and $u_* = (\langle u'w' \rangle^2 + \langle v'w' \rangle^2)^{1/4}$ [*McPhee*, 1992]. Decreasing the pump voltage from 12 to 6 Volts produced a 10% decrease in q, from 4.18 to 3.75 cm s^{-1}, and a ca. 14% decrease in $k/k_{100\%}$ of O_2, from 0.61 to 0.53 (Figure 3). Using the range of u_* measured with the ADV (0.4 – 0.8 cm s^{-1}), the turbulent lead number ranged from 0.5 to 0.15, i.e., significantly less than one, indicating that shear production from the submersible pumps dominated buoyant convection. There are few field measurements of turbulence beneath winter sea ice in the presence of leads, but *McPhee* [1992] reported measurements of q from 2.63 to 2.84 cm s^{-1} and u_* from 0.9 to 1.26 cm s^{-1} under drifting pack ice in the Arctic. These values are similar to the turbulence measured during the partial cover conditions of this experiment - the TKE in the tank was ca. 30% greater, and the estimate of friction velocity was smaller by 80% than the field measurements of *McPhee* [1992].

4. Conclusions

[14] Several of the complex physical processes that take place during the freezing of saltwater have been investigated using O_2 and SF_6 as conservative dissolved gas tracers of mass transport. Measurements of the gas exchange rate, k, during conditions of fractional ice cover indicate that gas flux through the ice pack may not scale linearly with the open water area. In these experiments turbulence beneath the ice was produced using submersible pumps, and a decrease in mixing by reduced pump power produced a decrease in TKE and a correspondent decrease in k, as expected. While the estimates of TKE in the tank were of similar magnitude to the measurements of TKE in the field beneath drifting ice by *McPhee* [1992], we don't expect that these experiments represent the range of turbulent conditions and processes beneath sea ice nor the magnitude of gas transfer through the ice pack. Instead, they indicate that an estimate of the effective gas flux through sea ice should account for turbulence and circulation processes under the ice. The limiting conditions of strong boundary layer flow and free convection that *Morison et al.* [1992] use to describe circulation beneath leads depict a renewal of water exposed to the opening in the ice, so that heat and mass transport through a lead may produce a larger "footprint" than is indicated by the surface area of open water.

[15] From the perspective of the dissolved gases in the surface layer of the ocean, the comparison of O_2 and SF_6 with salinity indicates that gas solutes are rejected from the ice more effectively than salt. The greater rejection of gases may be the result of faster gas diffusion away from the freezing interface into the region of water convection. Indeed, *Killawee et al.* [1998] observed a diffusive boundary layer for ionic solutes beneath growing ice. Comparing

the rejection of solutes in this study with a similar laboratory study involving CO_2 during freezing, high rejection efficiency is also observed for CO_2 and for total inorganic carbon (DIC) [*Nomura et al.*, 2006]. Those authors report that 66.9% of DIC in seawater that became sea ice was rejected to the underlying water volume, while comparatively little CO_2 was transferred from the ice to the air (0.8% of the initial CO_2 in frozen seawater). The combined effect of these processes, as well as the biological processes that take place within the ice [*Delille et al.*, 2007], determine the seasonal redistribution of DIC from the surface ocean, that occurs as a result of sea ice advance and retreat. These experiments offer some insight into the physical processes acting on dissolved gases during ice formation and deformation; the magnitude of these effects is an open question.

References

Arrigo, K. R., and G. L. Van Dijken (2007), Interannual variation in air-sea CO_2 flux in the Ross Sea, Antarctica: A model analysis, *J. Geophys. Res.*, *112*, C03020, doi:10.1029/2006JC003492.

Cox, G. F. N., and W. F. Weeks (1983), Equations for determining the gas and brine volumes in sea-ice samples, *J. Glaciol.*, *29*, 306–316.

Craig, H., R. A. Wharton, and C. P. McKay (1992), Oxygen supersaturation in ice-covered Antarctic Lakes: Biological versus physical contributions, *Science*, *255*, 318–321.

Delille, B., B. Jourdain, A. V. Borges, J.-L. Tison, and D. Delille (2007), Biogas (CO_2, O_2, dimethysulfide) dynamics in spring Antarctic fast ice, *Limnol. Oceanogr.*, *52*, 1367–1379.

Dieckmann, G. S., G. Nehrke, S. Papadimitriou, J. Göttlicher, R. Steininger, H. Kennedy, D. Wolf-Gladrow, and D. N. Thomas (2008), Calcium carbonate as ikaite crystals in Antarctic sea ice, *Geophys. Res. Lett.*, *35*, L08501, doi:10.1029/2008GL033540.

Golden, K. M., H. Eicken, A. L. Heaton, J. Miner, D. J. Pringle, and J. Zhu (2007), Thermal evolution of permeability and microstructure in sea ice, *Geophys. Res. Lett.*, *34*, L16501, doi:10.1029/2007GL030447.

Gosink, T. A., J. G. Pearson, and J. J. Kelly (1976), Gas movement through sea-ice, *Nature*, *263*, 41–42.

Ho, D. T., L. Bliven, R. Wanninkhof, and P. Schlosser (1997), The effect of rain on air-water gas exchange, *Tellus, Ser. B*, *49*, 149–158.

Killawee, J. A., I. J. Fairchild, J.-L. Tison, L. Janssens, and R. Lorrain (1998), Segregation of solutes and gases in experimental freezing of dilute solutions: Implications for natural glacial systems, *Geochim. Cosmochim. Acta*, *62*, 3637–3655.

Marion, G. M. (2001), Carbonate mineral solubility at low temperatures in the Na-K-Mg-Ca-H-Cl-SO_4-OH-HCO_3-CO_3-CO_2-H_2O system, *Geochim. Cosmochim. Acta*, *65*, 1883–1896.

Martinson, D. G. (1990), Evolution of the southern ocean winter mixed layer and sea ice: Open ocean deepwater formation and ventilation, *J. Geophys. Res.*, *95*, 11,641–11,654.

McPhee, M. (1992), Turbulent heat flux in the upper ocean under sea ice, *J. Geophys. Res.*, *97*, 5365–5379.

Morison, J. H., M. G. McPhee, T. B. Curtin, and C. A. Paulson (1992), The oceanography of winter leads, *J. Geophys. Res.*, *97*, 11,199–11,218.

Nomura, D., H. Yoshikawa-Inoue, and T. Toyota (2006), The effect of sea-ice growth on air–sea CO_2 flux in a tank experiment, *Tellus, Ser. B*, *58*, 418–426.

Papadimitriou, S., H. Kennedy, G. Kattner, G. S. Dieckmann, and D. N. Thomas (2003), Experimental evidence for carbonate precipitation and CO_2 degassing during ice formation, *Geochim. Cosmochim. Acta*, *68*, 1749–1761.

Richardson, C. (1976), Phase relationships in sea ice as a function of temperature, *J. Glaciol.*, *17*, 507–519.

Rysgaard, S., R. N. Glud, M. K. Sejr, J. Bendtsen, and P. B. Christensen (2007), Inorganic carbon transport during sea ice growth and decay: A carbon pump in polar seas, *J. Geophys. Res.*, *112*, C03016, doi:10.1029/2006JC003572.

Wanninkhof, R., J. R. Ledwell, W. S. Broecker, and M. Hamilton (1987), Gas exchange on Mono Lake and Crowley Lake, California, *J. Geophys. Res.*, *92*, 14,567–14,580.

Zappa, C. J., P. Raymond, E. Terray, and W. R. McGillis (2003), Variation in surface turbulence and the gas transfer velocity over a tidal cycle in a micro-tidal estuary, *Estuaries*, *26*, 1401–1415.

———————————

B. Loose, W. R. McGillis, P. Schlosser, and T. Takahashi, Lamont-Doherty Earth Observatory of Columbia University, 61 Route 9W, Palisades, NY 10964, USA. (brice@ldeo.columbia.edu)

D. Perovich, U.S. Army Corps of Engineers Cold Regions Research and Engineering Laboratory, 72 Lyme Road, Hanover, NH 03755-1290, USA.